Journal of Atmospheric and Terrestrial Physics, Vol. 45, No. 6, pp. 353–367, 1983.
Printed in Great Britain.

0021–9169/83 $3.00 + 0.00

Very-low frequency signals (2–10 kHz) received at Palmer Station, Antarctica, from the 21.4 km dipole antenna at Siple Station, 1400 km distant

S. TKALCEVIC

Space, Telecommunications and Radioscience Laboratory, Stanford University, Stanford, CA 94305, U.S.A.

(*Received in final form* 21 *December* 1982)

Abstract—Radio signals transmitted from the unique experimental VLF transmitter at Siple Station (76°S, 84°W), Antarctica, as well as VLF signals from communication and navigation systems and waves that propagate in the ionosphere and magnetosphere in the whistler mode, are regularly received and analysed at Palmer Station (65°S, 64°W), Antarctica. The amplitude and polarization properties of the Siple signals are predicted using a ray optics analysis. The amplitude of the signal received from Siple varies with frequency; observed nulls in the signal spectrum, where the signal amplitude falls 5–10 dB below what might be expected, are explained by the ray analysis. The amplitude spectrum is observed to be very sensitive to ionospheric conditions. Whereas the arrival bearings of signals from VLF transmitters other than Siple are found to be within 5° of their expected values, which is consistent with their expected vertical polarization and the operation of the DF system, an approximately 90° anomaly in the apparent arrival bearing of the signals from Siple is attributed to the essentially horizontal polarization of the received signal. The anomaly is found to be consistent with the theory of operation of the DF system. Occasional anomalies greater than 90° are explained in terms of a combination of polarization error and a smaller multi-path error. Siple two-hop signals and whistlers propagating on a common magnetospheric path showed arrival bearings and other properties consistent with a path end point within 200 km of Siple. This suggests that these signals were received at Palmer with essentially vertical polarization.

1. INTRODUCTION

Very-low-frequency (VLF) radio observing facilities were established at Palmer Station (65°S, 64°W), Antarctica, in 1978. One of the experiments involves using a frequency-tracking direction finder (DF) receiver (LEAVITT, 1975) to monitor the direction of arrival of various VLF signals. There are two main groups of monitored signals, those that propagate only in the earth–ionosphere waveguide, and those that propagate in the magnetosphere and then enter the waveguide. The polarization of signals confined to the waveguide is a function of the source polarization, path length, ionospheric height and density, as well as the ground permittivity and conductivity. On the other hand, signals propagating through the magnetosphere excite the earth–ionosphere waveguide with circularly polarized waves regardless of the original source polarization and the received wave will in general show elliptical polarization.

Examples of the 'waveguide only' group are signals from the experimental VLF transmitter at Siple Station (76°S, 84°W), Antarctica (HELLIWELL and KATSUFRAKIS, 1978) and various OMEGA station signals. The 'magnetospheric' group includes both natural whistlers and signals injected by the Siple transmitter. The DF studies of these whistler-mode signals are of particular interest because they may yield information about the location and dynamics of duct exit points.

The accuracy of the DF system at Palmer Station depends on the characteristics of the received signals. Therefore, the direction of arrival information must be analysed carefully in order to deduce correct values of bearing from the measured data. The two groups of signals mentioned above represent a wide range of wave properties. Siple station is unusual in that it is a source of horizontally polarized waves, while Omega stations transmit vertically polarized waves, and whistler signals from the magnetosphere represent a source of circularly polarized waves. These three different types of signal may be used to study the operation of the DF system at Palmer as well as to investigate propagation in the earth–ionosphere waveguide.

DF measurements at Palmer of the direct signals from the Siple VLF transmitter contain a very large apparent error (BILLEY, 1981), of the order of 60–90° with respect to the great circle bearing. This large error can be explained in terms of systemic (or polarization) error of the DF system. The error has been reproduced by simulating Siple signal propagation in calculations analogous to those of CRARY (1961), STRANGEWAYS (1980), and STRANGEWAYS and RYCROFT (1980), who used whistler-mode signals as the source. The results of the numerical modeling are in good agreement with

both the measured amplitude and direction of arrival of the Siple signal.

Measurements at Palmer show that the amplitude of the Siple direct signal may vary rapidly with frequency and that the signal amplitude for a given frequency may change within a short time interval (approximately 10 min) during sunrise. Computations using the ray method of analysis support these results.

2. RADIATION FROM THE HORIZONTAL DIPOLE AT SIPLE

Whereas most VLF transmitters use vertical antennas, designed to produce ground wave and ionospherically reflected signals, the VLF transmitter at Siple Station uses a 21.4 km long horizontal dipole designed to radiate upwards to excite whistler-mode signals. The 2 km thick ice layer beneath the antenna acts as a lossy dielectric and provides a significant separation between the antenna and the conductive ground to permit upwards radiation. The input impedance of the dipole as computed by RAGHURAM *et al.* (1974) is in good agreement with measured values, but the radiation pattern has not been calculated. Such a calculation is complicated by the multi-layer nature of the medium (stratified ice slab above ground of unknown conductivity).

The theoretical approach used in this study was to remove the ice layer and to assume that the dipole is in free space 2 km above ground. To compensate for the removal of the ice layer, it was necessary to change the antenna wire diameter and to choose values of both the ground permittivity and conductivity in order to make the computed input impedance consistent with measurements. The results of the computations show that the radiation pattern does not change significantly over the frequency range considered here. Therefore the pattern computed at 5 kHz is taken to represent the antenna radiation properties. Figure 1(a) shows the azimuthal radiation pattern at 30° elevation when

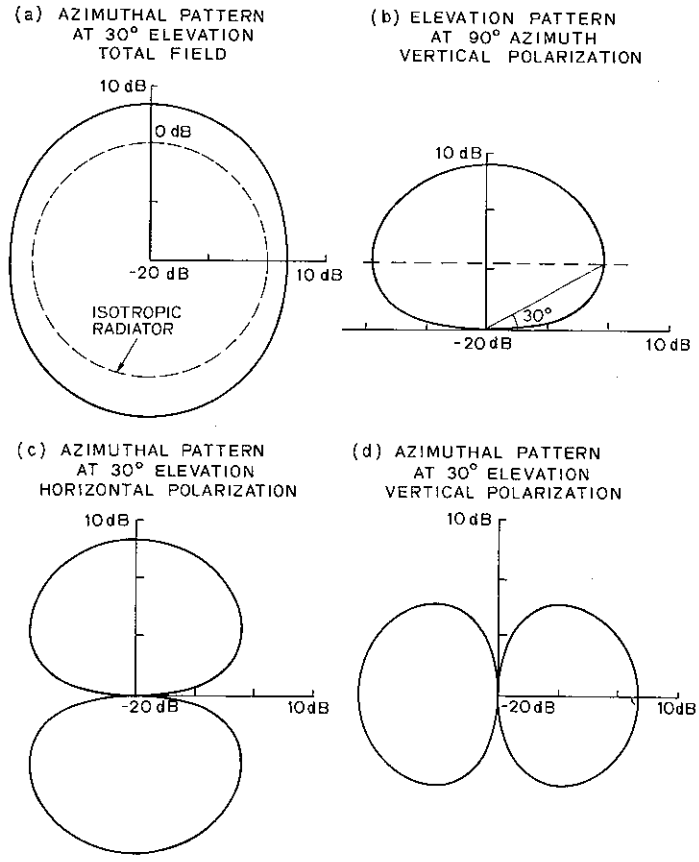

Fig. 1. Radiation patterns of Siple 21.4 km long horizontal dipole antenna. Dipole gain is given relative to an isotropic radiator as indicated by the dashed line in (a). In (a), (b), (c) and (d) the dipole is oriented along the horizontal coordinate axis.

the dipole is aligned with the horizontal coordinate axis. Figure 1(b) shows the elevation pattern for broadside radiation (perpendicular to the dipole). In Fig. 1(a) both horizontally and vertically polarized components are added together to give the total radiated field. Figures 1(c) and (d) show separately the horizontally and vertically polarized components associated with Fig. 1(a).

Palmer Station is located directly broadside to the Siple dipole antenna. Figure 1 indicates that waves launched in this direction are purely horizontally polarized (while waves in the end-fire direction are purely vertically polarized, and waves in intermediate directions are elliptically polarized).

The antenna efficiency as a function of frequency has been estimated by RAGHURAM *et al.* (1974). In the present work, the following approximation to RAGHURAM *et al.* result for the antenna efficiency was used in computations for frequencies between 3 and 9 kHz:

$$\eta = 4.234 - 3.036f + 0.69f^2 - 0.0385f^3 \qquad (1)$$

where η is the antenna efficiency, and f is the frequency in kHz.

The antenna efficiency varies from 0.4% at 3 kHz up to 4.6% at 9 kHz.

3. CALCULATIONS OF FIELD STRENGTH AT THE RECEIVER

In general there are two methods available for field strength computations of VLF waves propagating in the earth–ionosphere waveguide, the 'ray method' and the 'mode method'. The first method uses the principles of geometrical optics for reflection from sharp boundaries, while the second method is based on solving Maxwell's equations for the boundary conditions in the waveguide. Each method should produce the same results, but it is preferable to use the ray method for short distances, with the mode method being more suitable for long propagation distances. The most important factor governing the choice of methods is the number of rays vs number of modes needed to compute the field strength for a given length of propagation path. The distance between Siple and Palmer is 1440 km, which favors use of the ray method. It was found that it is sufficient to use the first 15 rays to achieve high precision in the field computations; the addition of the 16th ray changes the total computed field strength by less than 1%, for all the computations presented here.

The ray method computations were further simplified by the following assumptions:

(a) The ionosphere is represented by a homogeneous layer with a sharp lower boundary.

(b) Refractive indices are derived using the QL approximation.

(c) The ground along the Siple–Palmer path is represented by a two layer model, with a 2 km thick ice layer lying over poorly conducting ground.

(d) The reflection coefficients are derived assuming that the ionosphere and ground are flat reflectors. The curvature of the Earth and ionosphere is applied only to compute the path lengths of the rays.

(e) The free space attenuation of a wave is inversely proportional to the distance it travels.

An example of the ray path geometry used is given in Fig. 2.

With the above assumptions, the ionosphere can be described in terms of its refractive indices, which are given by BUDDEN (1961) and WAIT and PERRY (1957):

$$\mu^2 = 1 - i(\omega_r/\omega)\exp(\pm i\tau) \qquad (2)$$

where

$$\tan\tau = \omega_L/\nu \qquad (3)$$

and

$$\omega_r = \omega_0^2/\sqrt{\nu^2+\omega_L^2}, \qquad (4)$$

$$\omega_0 = \frac{Ne}{\varepsilon_0 m}, \qquad (5)$$

$$\omega_L = eB/m, \qquad (5a)$$

N is the number of electrons per cubic meter, $\varepsilon_0 = 8.854 \times 10^{-12}$, ν is the electron collision frequency, B is the Earth's magnetic field strength, and e and m are the charge and mass of the electron, respectively.

Using the refractive indices given by equation (2) it is possible (BUDDEN, 1951) to evaluate the four ionospheric reflection coefficients ${}_{\perp}R_{\perp}$, ${}_{\perp}R_{\parallel}$, ${}_{\parallel}R_{\parallel}$ and ${}_{\parallel}R_{\perp}$ required for the field strength computations. The first subscript denotes the polarization of the incident wave ($\perp$ for horizontal polarization, with the E field perpendicular to the plane of incidence, and $\parallel$ for vertical polarization, with the E field in the plane of

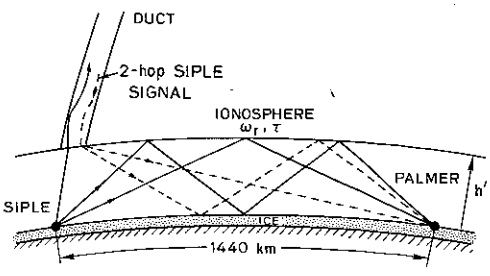

Fig. 2. Siple–Palmer path geometry showing multiple wave reflections in the earth–ionosphere waveguide.

incidence); the second subscript gives the polarization of the reflected wave. These four reflection coefficients were expressed in a form suitable for calculations by WAIT and PERRY (1957), and the expressions developed by them were used in the calculations.

To compute the field strength of a particular ray it is also necessary to evaluate the Fresnel reflection coefficients $Rg_{\parallel}$ and $Rg_{\perp}$, which characterize the reflective properties of the ground. These coefficients are computed using a two layer model of the ground, in which the top layer is an ice slab 2 km thick with relative dielectric constant $\varepsilon_r = 5-\mathrm{i}\,10$. The bottom layer is semi-infinite, with conductivity $\sigma = 0.001$ mhos m^{-1} and relative dielectric constant $\varepsilon_r = 10$.

Electric fields of the nth ray may be evaluated using the above reflection coefficients, as follows:

$$\begin{bmatrix} E_{\perp}^{(n)} \\ E_{\parallel}^{(n)} \end{bmatrix} = \frac{e^{i\phi}}{R_n} \left\{ \begin{bmatrix} {}_{\perp}R_{\perp} & {}_{\parallel}R_{\perp} \\ {}_{\perp}R_{\parallel} & {}_{\parallel}R_{\parallel} \end{bmatrix} \begin{bmatrix} Rg_{\perp} & 0 \\ 0 & Rg_{\parallel} \end{bmatrix} \right\}^{n-1} \cdot \begin{bmatrix} {}_{\perp}R_{\perp} & {}_{\parallel}R_{\perp} \\ {}_{\perp}R_{\parallel} & {}_{\parallel}R_{\parallel} \end{bmatrix} \begin{bmatrix} E_{\perp s} \\ E_{\parallel s} \end{bmatrix} \quad (6)$$

where n is the order of the ray (n ionospheric reflections; $n-1$ ground reflections), R_n is the propagation distance for the nth ray, $\phi_n = -2\pi R_n f/c$, the phase of the nth ray, $E_{\perp s}$ is the horizontally polarized component of the source electric field, and $E_{\parallel s}$ is the vertically polarized component of the source electric field.

With the help of equation (6), the total electric field at the receiver is calculated by adding the appropriate number of rays (15, as noted above).

It was not necessary to include a ground wave in computations of the total field at the receiver, because a horizontally polarized ground wave is very heavily attenuated, even for poorly conducting ground along the signal path.

Each ray (see Fig. 3) arrives at the receiver at a different vertical angle β_n, depending on the transmitter–receiver distance and on the ionospheric height. Therefore, the three electric field components at the receiver are (CRARY, 1961):

$$\bar{\varepsilon}_x = -\sum_n E_{\perp}^{(n)}, \quad (7)$$

$$\bar{\varepsilon}_x = -\sum_n E_{\parallel}^{(n)} \cos \beta_n, \quad (8)$$

$$\bar{\varepsilon}_z = \sum_n E_{\parallel}^{(n)} \sin \beta_n, \quad (9)$$

where $E_{\parallel}^{(n)}$ and $E_{\perp}^{(n)}$ are the electric field components of the nth ray calculated using equation (6). The coordinate system used is shown in Fig. 3.

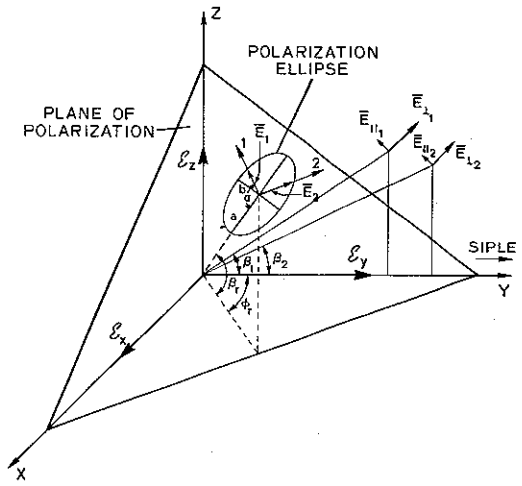

Fig. 3. Observing geometry at Palmer showing the plane of polarization of a wave that results from summing the contributions of multiple Siple–Palmer raypaths.

Equations (7)–(9) may be rewritten as:

$$\bar{\varepsilon}_x = E_x \sin(\omega t + \gamma_1), \quad (10)$$

$$\bar{\varepsilon}_y = E_y \sin(\omega t + \gamma_2), \quad (11)$$

$$\bar{\varepsilon}_z = E_z \sin(\omega t + \gamma_3), \quad (12)$$

where E_x, E_y, and E_z are the magnitudes and γ_1, γ_2, and γ_3 are the phases of the three field components.

It can be shown (MORGAN and EVANS, 1951; CRARY, 1961) that the resultant field represented by the three mutually orthogonal sinusoidal components given by equations (10)–(12) is an elliptically polarized wave. The polarization ellipse parameters, as well as the orientation of the polarization plane, are then given in terms of E_x, E_y, E_z, γ_1, γ_2, and γ_3. Note that the plane of incidence of the resultant wave (plane obtained by rotating z–y plane by ϕ_r degrees, Fig. 3) does not in general coincide with that of the component waves (z–y plane in Fig. 3). Furthermore, the E field and H field polarization ellipses are contained in different planes. Our calculations were actually done for H, since the response of the Palmer DF system used to observe the signal is in terms of the H field components.

Using Fig. 3 and the results derived by MORGAN and EVANS (1951), it follows that for the E field (similarly for the H field),

$$\tan \phi_r = \frac{E_x \sin \gamma_1}{E_y \sin \gamma_2}, \quad (13)$$

$$\tan^2(90-\beta_r = \frac{E_x^2 E_z^2 \sin^2(\gamma_1-\gamma_3) + E_y^2 E_z^2 \sin^2(\gamma_3-\gamma_2)}{E_x^2 E_y^2 \sin^2(\gamma_2-\gamma_1)} \quad (14)$$

and

$$\bar{\varepsilon}_1 = \frac{E_y + \dfrac{E_z}{\sin \beta_r} \sin \phi_r}{\cos \phi_r} = E_1 \sin(\omega t + \delta_1), \quad (15)$$

$$\bar{\varepsilon}_2 = \frac{E_z}{\sin \beta_r} = E_2 \sin(\omega t + \delta_2) \quad (16)$$

where ϕ_r and β_r define the orientation of the polarization plane, while $\bar{\varepsilon}_1$ and $\bar{\varepsilon}_2$ define the polarization ellipse locus which lies in that plane (plane 1–2 in Fig. 3).

Finally, using E_1, E_2, δ_1 and δ_2 it is possible to find the ellipse axes, the axis ratio R and the tilt angle of the major axis. These parameters (R and α), together with the elevation angle β_r (equation (14)) are then used to calculate the direction of arrival error $\Delta\theta$ using equation (25) in the second section following.

The ellipse major axis a, the minor axis b, and the tilt angle α, evaluated in terms of E_1, E_2, δ_1 and δ_2, are

$$\alpha = \tfrac{1}{2} \arctan\left[\frac{2E_1E_2 \cos(\delta_2 - \delta_1)}{E_1^2 - E_2^2}\right] \quad (17)$$

$$a = \sqrt{[E_1 \cos\alpha + E_2 \cos(\delta_2 - \delta_1) \sin\alpha]^2 + E_2^2 \sin^2(\delta_2 - \delta_1) \sin\alpha}, \quad (18)$$

$$b = \sqrt{[E_1 \sin\alpha - E_2 \cos(\delta_2 - \delta_1) \cos\alpha]^2 + E_2^2 \sin^2(\delta_2 - \delta_1) \cos\alpha}, \quad (19)$$

and the axis ratio R is

$$R = b/a \quad (R \leqslant 1). \quad (20)$$

As noted, the arrival angle of the composite wave (Fig. 3) differs from that of the individual rays. Thus multi-path propagation will be a source of error when measuring the direction of arrival. This effect, known as multi-path error, may be calculated by applying equation (13) to the H field components (the Palmer DF antennas measure H_x and H_y). This gives the azimuth ϕ_r of the normal to the plane of polarization, and thus the apparent arrival bearing. At the same time there is also a polarization error, which depends upon the type of DF receiver used. STRANGEWAYS (1980) and STRANGEWAYS and RYCROFT (1980) discuss multi-path and polarization errors in different DF systems, including the crossed loops goniometer (BULLOUGH and SAGREDO, 1973), the A and B methods (COUSINS, 1972), the field analysing method (OKADA *et al.*, 1977), the NPE (no polarization error) method (TSURUDA and HAYASHI, 1975), and the LEAVITT frequency tracking direction finder (LEAVITT *et al.*, 1978).

We shall now present numerical and experimental results for Siple–Palmer propagation.

4. NUMERICAL RESULTS

The numerical analysis of Siple–Palmer propagation was done for the three different ionospheric models as listed in Table 1.

Table 1

	Model I	Model II	Model III
ω_r	5×10^5	1.5×10^6	6×10^5
τ	60°	15°	15°
h'	90 km	70 km	70 km

τ and ω_r are as given by equations (3) and (4), while h' represents the vertical height of ionospheric reflection. The computational results can be separated into three major groups:

(a) electric field calculations;
(b) polarization error calculations;
(c) multi-path error calculations.

Figure 4(a) shows the amplitude of the E_x field component for all three ionospheric models as a function of frequency. Similarly, Fig. 4(b) shows the amplitude of the E_y field component, and Fig. 4(c) shows the amplitude of the E_z component. The multi-path error is shown in Fig. 4(e). In all these calculations it was assumed that the $E_{\parallel s}$ term in equation (6) is equal to zero. This is a reasonable assumption for Siple–Palmer propagation. The maximum power delivered to the antenna used in the calculations was 34 kW at $f_0 = 5000$ Hz; the power delivered at lower frequencies was less, falling off as f/f_0 due to the characteristics of the transmitter tuning circuit.

In order to show the effects of the dipole radiation pattern (Fig. 1) the amplitude of the E_z component for the dipole antenna and for an isotropic radiator were compared using Model I for the ionosphere. The results are shown in Fig. 4(f). Typical ray field strengths for the dipole antenna and an isotropic radiator, normalized to the amplitude of the 4-hop ray, are given in Fig. 5.

A discussion of these numerical results will be presented after the section on the results of measurements.

5. DIRECTION FINDING RECEIVER SYSTEM

The VLF receiving system at Palmer station includes a frequency-tracking direction finder designed by

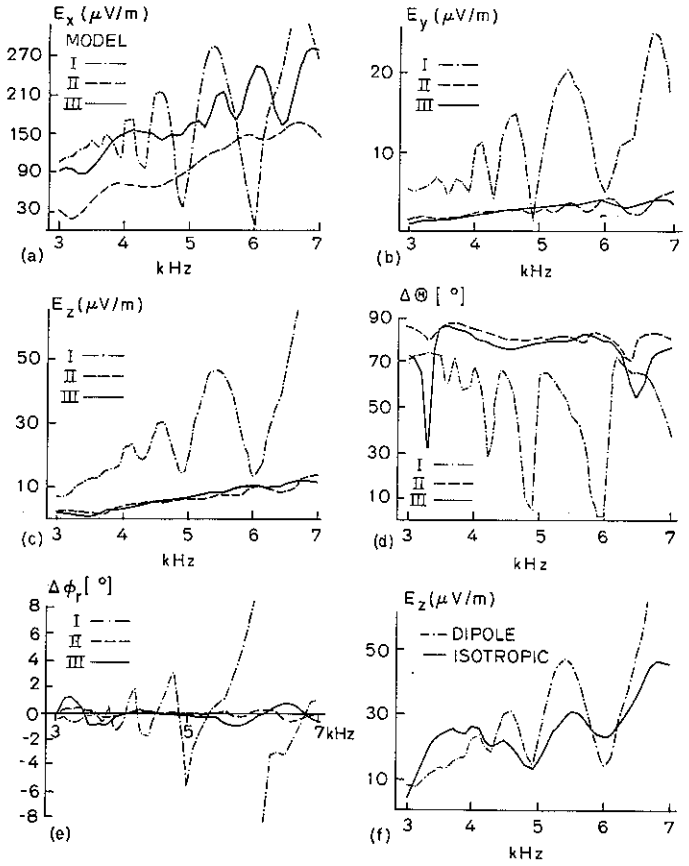

Fig. 4. Numerical results showing expected field strengths E_x, E_y, and E_z of Siple signals at Palmer. Also shown are expected values of the polarization error $\Delta\theta$, and the multi-path error $\Delta\phi_r$. Calculations are done for three different ionospheric models as indicated: — · — Model I; ——— Model II; ——— Model III.

LEAVITT (1975). This DF system uses crossed loops and a vertical monopole to measure, respectively, the wave field components H_x, H_y, and E_z. The X-axis direction coincides with the north–south direction in the geomagnetic coordinate system and the Y-axis with the east–west direction.

Theoretically one needs to know all six field components in order to determine the azimuth and elevation angles of an incoming signal. The technique is to compute the Poynting vector components,

$$P_x = E_y H_z - E_z H_y, \tag{21}$$

$$P_y = E_z H_x - E_x H_z, \tag{22}$$

$$P_z = E_x H_y - E_y H_x \tag{23}$$

and then determine the direction of arrival.

However, if the purpose of the DF system is to measure the azimuth angle alone, only P_x and P_y need to be measured. In this case the angle of arrival is given as (LEAVITT, 1975)

$$\theta = \arctan(P_y/P_x). \tag{24}$$

The DF system discussed by LEAVITT *et al.* (1978) does not measure the H_z, E_x, or E_y components of the wave's field, all of which are needed to calculate P_x and P_y. Thus the best results will be achieved either if H_z is small or if both E_x and E_y are small. LEAVITT (1975) gives a more detailed discussion in which he predicts that the Palmer DF system will produce the best results with signals polarized in the plane of incidence and incident at relatively low elevation angles. For other types of signals the probability of error increases, with the size of the error dependent upon the polarization and elevation angle of arrival of the signals. The polarization error for the Palmer DF system is given as

$$\Delta\theta = \arctan\left(\sin\beta_r \frac{(R^2-1)\cos\alpha\sin\alpha}{\cos^2\alpha + R^2\sin^2\alpha}\right) \tag{25}$$

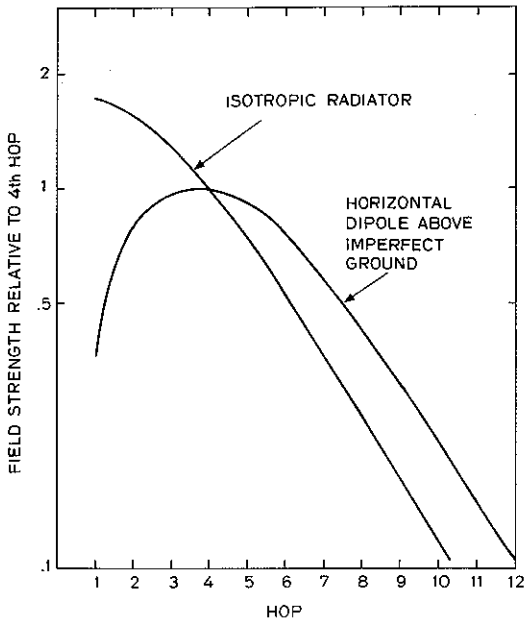

Fig. 5. Individual ray field strengths at Palmer for the Siple dipole antenna and isotropic radiator, normalized to the amplitude of the four-hop ray.

where (Fig. 3) β_r is the elevation angle of arrival, R is the polarization ellipse axis ratio, and α is the tilt angle of the major axis of the polarization ellipse.

If the above parameters of a received signal can be estimated, equation (25) can be used to calculate the polarization error. As shown in Fig. 4(d), this is close to 90° throughout the frequency range for Models II and III and shows wide excursions for Model I.

6. RESULTS OF MEASUREMENTS

Measurements with the DF system at Palmer on direct signals from Siple show a large error when compared with the great circle bearing from Siple. Figure 6 shows measurements which illustrate typical behavior of the DF error as a function of both frequency and time. These results were obtained from measurements made over a period of 36 h, during which the direction of arrival was measured every 20 min at 7 different frequencies between 3.5 and 6.5 kHz in steps of 0.5 kHz. The DF error at any given frequency is represented by the average value computed over the time periods indicated in Fig. 6. The fluctuations in the direction of arrival are plotted as vertical bars which represent the standard deviation in the measurements. [There is a missing data point at 6 kHz in Fig. 6(c) caused by a very weak signal for which it was impossible to measure the direction of arrival.]

A detailed data set from 3 July 1978 includes measurements of both Siple signal amplitude and direction of arrival. The transmitter format on that day included falling frequency ramps, frequency staircases and CW signals. The falling frequency ramp and frequency staircase signals shown in Fig. 7 were repeated every 5 min for 4 h. Using those data, it was possible to determine field strength and direction of arrival as a function of frequency.

Figure 8 shows the results of DF measurements for the falling frequency ramp at 1306 UT. Starting from

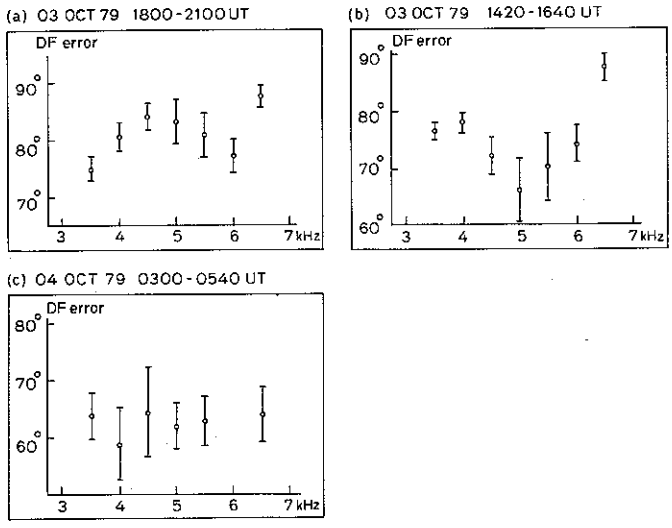

Fig. 6. Direction of arrival error measured for Siple signal at Palmer over a 36 h period and signal frequency range 3.5–6.5 kHz.

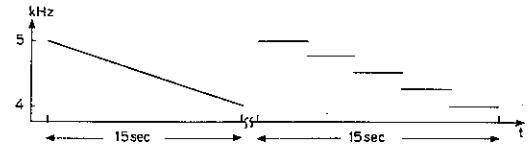

Fig. 7. Siple transmitter format used in amplitude and direction of arrival studies.

the top, the panels represent broad band VLF (3–6 kHz), DF receiver tracking filter frequency, DF receiver direction of arrival output, and DF receiver signal strength output. Figure 8(c) shows that the measured direction of arrival of the Siple direct signal is almost due west (in local geomagnetic coordinates), while the true bearing is due south. At 1306:18 UT and 1306:29 UT the direction of arrival (third panel, Fig. 8c) was north of west, indicating the presence of DF error larger than 90°. The amplitude variations of 10–12 dB are best seen as an intensity modulation on the VLF record (top panel, Fig. 8a), being less pronounced on the amplitude chart (bottom panel, Fig. 8d) due to the logarithmic scale. For purposes of comparison Fig. 9 shows the same signal 45 min later. By this time both the DF error and the amplitude signature of the signal have changed. The DF reading is mostly south-west, indicating a smaller DF error.

The changes in amplitude of the received Siple signals are illustrated by a series of amplitude spectrograms (Fig. 10). These spectrograms show the signal amplitude variations as a function of frequency at five different times. The dashed curve in Fig. 10(a) shows the expected amplitude variation due to transmitter tuning and antenna efficiency only; the effects of multi-path propagation are not included. The first three spectrograms (Figs. 10 a–c) were taken within a 0.5 h period and have the same general shape: a maximum field strength of about 20 μV m^{-1} at 5 kHz and a second peak at approximately 4.65 kHz. On the other hand, spectrograms taken at 1346 UT (Fig. 10d) and at 1351 UT (Fig. 10e) have different shapes. Figures 10(c)–(e) span a sunrise period near Palmer, when the

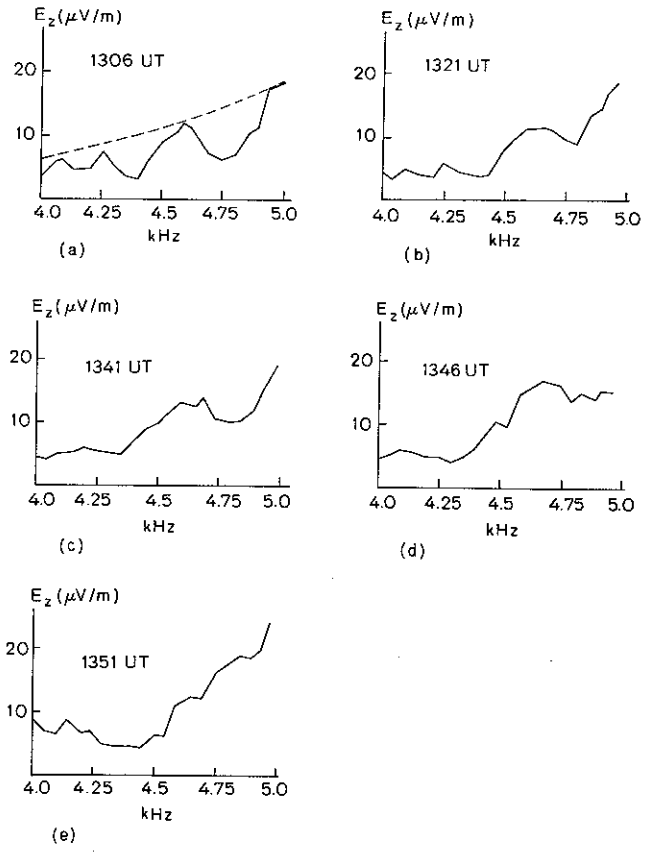

Fig. 10. Palmer amplitude measurements of Siple ramp signals within a 1 h period illustrating signal amplitude variations with frequency and time.

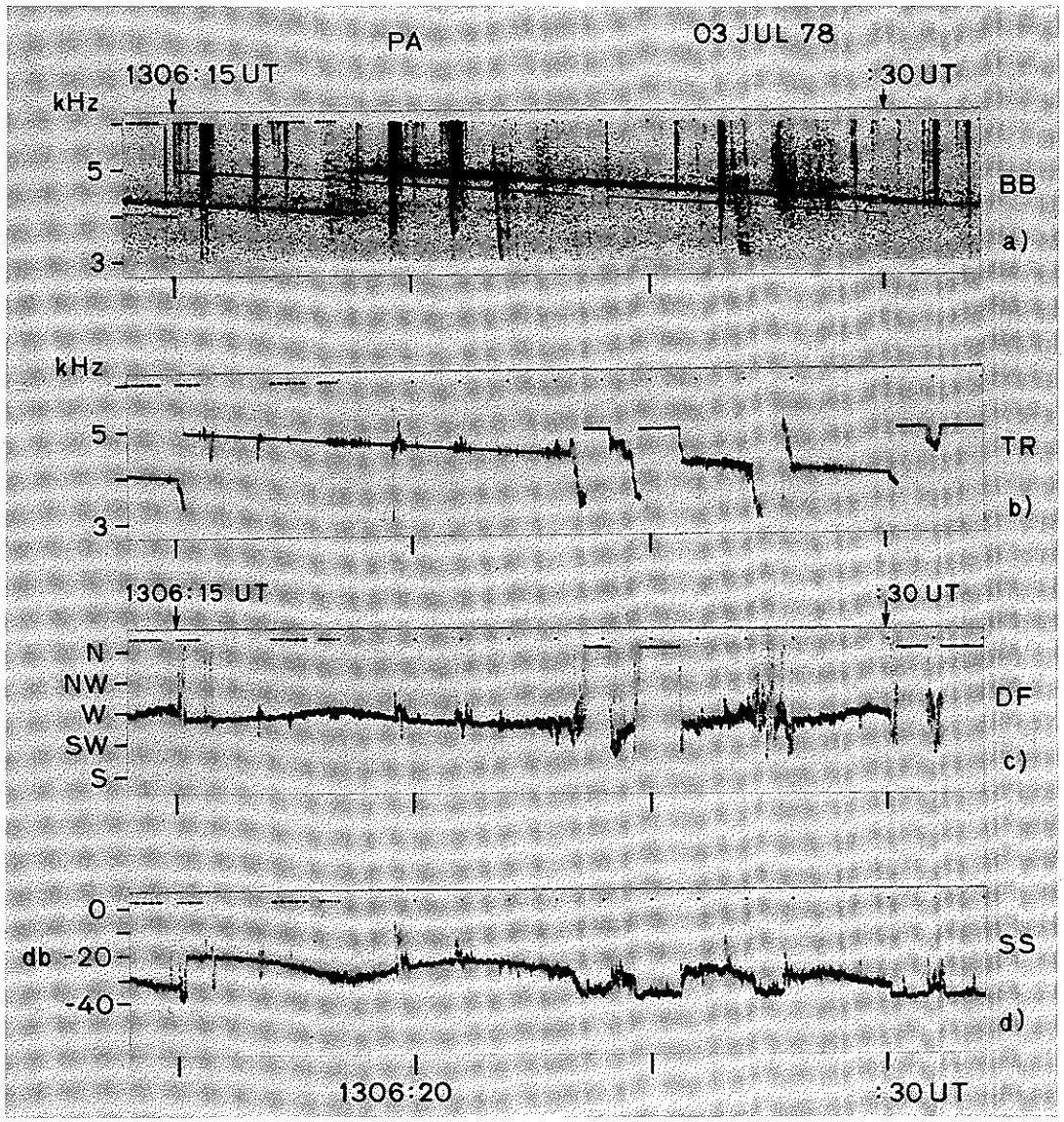

Fig. 8. Palmer measurements of Siple frequency-ramp signals on 3 July 1978 at 1306 UT, showing broad band VLF recording, DF tracking filter frequency, DF receiver direction of arrival, and DF receiver signal strength outputs.

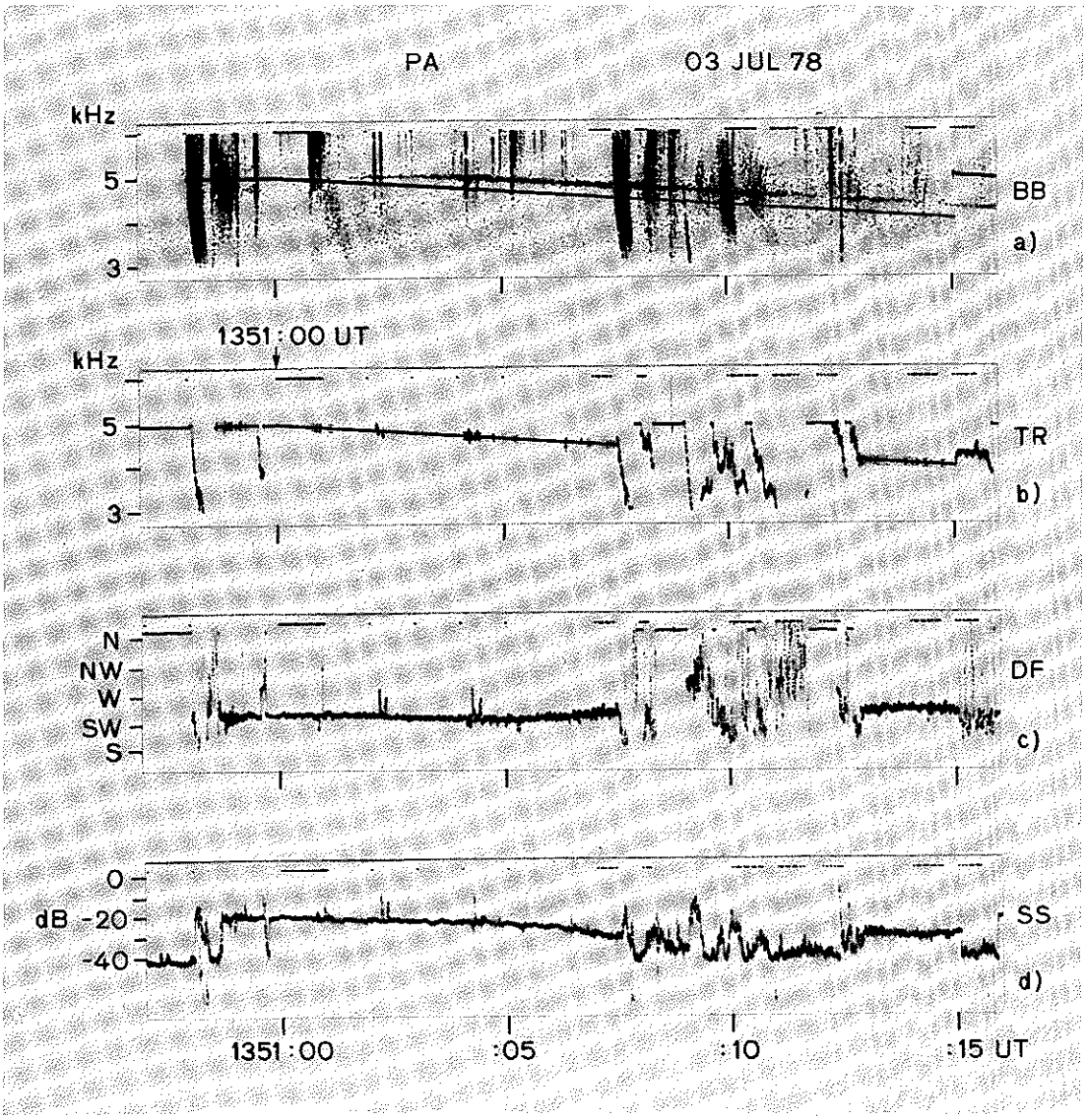

Fig. 9. Palmer measurements of Siple ramp signal at 1351 UT on 3 July 1978.

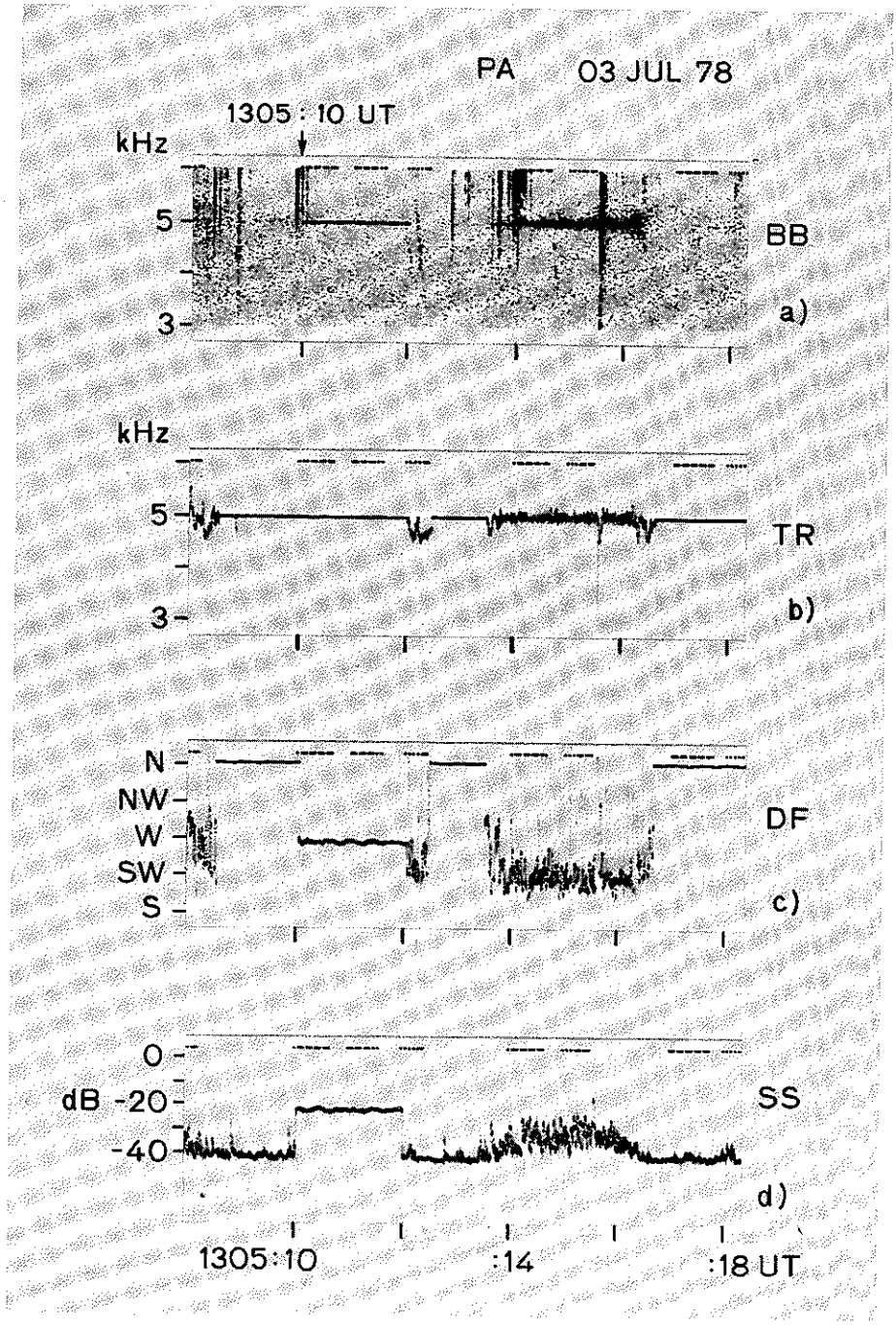

Fig. 11. Direct and two-hop Siple signals received at Palmer at 1305 UT on 3 July 1978.

enhancement of ionospheric ionization levels can be expected to affect the amplitude of Siple signals.

Figure 11 shows the results of DF measurements on a direct Siple signal (pulse at 1305:10 UT) and a 2-hop signal (1305:14 UT). The two-hop signal is longer than the transmitted pulse, indicating multi-path propagation. However, a portion of the signal approximately equal in length to the transmitter pulse could be consistently identified because of its higher amplitude. The arrival bearing of this section of the signal, slightly west of south, was found to agree with that of one of the components of multicomponent whistlers of that period, such as the examples in Fig. 9 at 1351:07 and 1351:10 UT. The one-hop magnetospheric travel times at the transmitter frequency of the two types of signal also agree, indicating that the whistler components and the prominent Siple signal followed a common path (CARPENTER and MILLER, 1976). The path endpoint was then located by the method of SEELY (1977), whereby the nose frequency information from the whistlers yields path L value, $L = 4.1 \pm 0.10$ in this case, which is then combined with the DF results. The result of the triangulation is shown in Fig. 12; the shaded area shows the estimated location of the duct, and allows for uncertainties in the measurements of the L-shell value and direction of arrival.

Previous work suggests that strong Siple signal propagation to the conjugate ground station should be concentrated on paths beginning within 200 km of the station (CARPENTER and MILLER, 1976; LEAVITT *et al.*, 1978; CARPENTER, 1980). Since the estimated signal path endpoint agrees with these results, we suggest that the actual exit point was located within 200 km of Siple, and that any systematic bearing error in the Siple 2-hop signals is much smaller than that of the direct signal.

Finally, 1978 measurements at Palmer of arrival bearings for various other VLF transmitters are presented in Table 2.

Table 2

Source	True bearing	Measured bearing
NPG	318.5°	318°
NAA	357.6°	358°–01°
Omega, Hawaii	276.2°	272°
Omega, ND	334.8°	331°
Omega, La Reunion	124.8°	123°
Omega, Argentina	357.8°	358°

The maximum DF error is less than 5°. Such a small error is expected, because signals from these sources are vertically polarized and the distances are large. As mentioned above, this type of signal is not expected to produce polarization error in the DF system at Palmer. This is also a good test of the DF system accuracy and calibration.

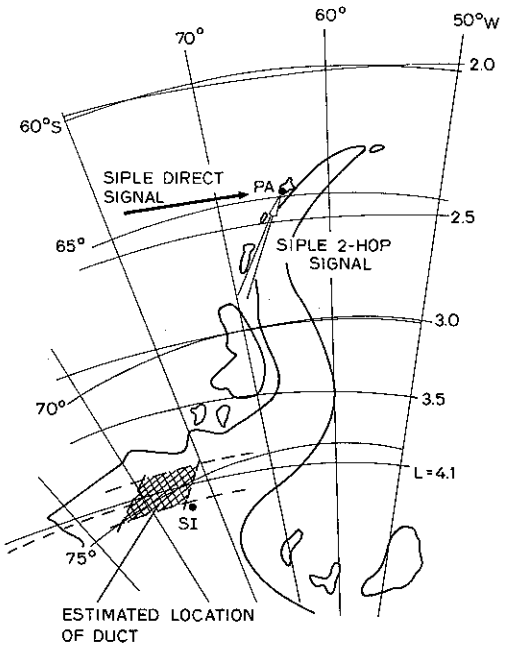

Fig. 12. Triangulated location of the estimated exit point of the magnetospheric duct shared by the prominent Siple whistler-mode signal and a whistler component on 3 July 1978.

7. DISCUSSION

We have presented both theoretical and experimental DF results for the VLF signal at Palmer after propagation from Siple. The large apparent error in measurements of the direction of arrival at Palmer (Figs. 8 and 9) is attributed mostly to the systemic polarization error of the DF system (Fig. 4d), since the multi-path error (Fig. 4e) is far smaller. However, Fig. 8(c) (DF panel) shows that the apparent bearing of the Siple signal is occasionally north of west (at 1306:19 and 1306:29 UT), which means that the DF error is occasionally larger than 90°. To explain this error of approximately 102° it is necessary to include multi-path error because polarization error is bounded between −90 and +90° (LEAVITT, 1975; LEAVITT *et al.*, 1978). It should be mentioned that the multi-path error can be very large for some propagation distances and source polarizations, although in typical cases it is expected to be opposite in sign to polarization error, thus reducing the effect of the latter (STRANGEWAYS, 1980; STRANGEWAYS and RYCROFT, 1980).

The amplitude measurements (Fig. 10) give the amplitude of the E_x field component, which is also

computed and shown in Fig. 4(c). Comparing Figs. 4(c) (dash-dot curve) and 10(a) we see good agreement between measurements and calculations for the nighttime ionosphere. Figures 4(c) (solid or dashed curve) and 10(e) are similar in shape but have different amplitudes, even though all of the measurements and computations were made for daytime ionospheric conditions. This may be due to ionospheric conditions along the path; a small portion of the path within about 350 km of Palmer was in daylight, but the rest of the path was always in darkness. Also note that the ice layer is not perfectly uniform as assumed, which will then also affect the results.

As noted in the previous section, the location of a duct end-point can be determined using a triangulation procedure. However, the DF information obtained from whistlers is also subject to errors, both polarization and multi-path. Therefore the accuracy of the location method will be limited by the accuracy of the error estimation. A possible way to determine a more exact location of a duct end-point would be to compute the DF error using procedures given by STRANGEWAYS (1978) and to correct the measured values. The accuracy of the measurements can also be improved by using an additional averaging of the bearings over frequency ranges of interest as suggested by COUSINS (1972). Although LEAVITT's system is not free of polarization errors, it has the advantage that it uses a narrow bandwidth frequency tracking filter that follows frequency changes of the signal and simultaneously reduces the system noise level.

The amplitude response, as illustrated in Fig. 10, might be used not only to observe frequency diversity and to optimize reception of VLF signals, but also as a remote sensing tool for changes in the ionosphere, where the frequencies of amplitude minima are directly related to ionospheric conditions.

8. CONCLUSIONS

We have studied the direction of arrival and amplitude behavior of various VLF signals using the direction finding receiver at Palmer Station, Antarctica. The results of those studies are summarized as follows:

(1) The amplitude and polarization properties of Siple, Antarctica, transmitter signals received 1440 km away at Palmer Station in a direction broadside to the antenna can be understood in terms of a ray optics analysis.

(2) The Siple transmitter signal, as received at Palmer, is essentially horizontally polarized. As a result, there is an approximately 90° anomaly in the apparent arrival bearing as indicated by the VLF direction-finding receiver at Palmer. This error is consistent with the theory of operation of the DF system.

(3) Occasional Siple transmitter signal arrival bearings with anomalies greater than 90° at Palmer can be understood as a combination of the polarization error noted above and a usually smaller multi-path error associated with the multiple rays that make up the received Siple signal.

(4) The arrival bearings of signals from fixed frequency VLF transmitters (Omegas, NAA, NPG) propagating in the earth–ionosphere waveguide to Palmer are within five degrees of the expected values. This is consistent with their expected vertical polarization and the theory of operation of the DF system.

(5) In one case, two-hop Siple signals and whistlers showed an arrival bearing consistent with a path exit point from the ionosphere within 200 km of Siple, as expected from previous studies of path locations. This suggests that the polarization error associated with these signals is small and that the polarization of the signals, as received at Palmer, is close to vertical.

(6) Siple signal amplitude behavior at Palmer may vary as a function of frequency. Variation of the type observed (5–10 dB) are predicted by a ray analysis. The observations suggest that the amplitude spectra are very sensitive to ionospheric conditions along the path.

Acknowledgements—I thank R. HELLIWELL, D. CARPENTER and J. KATSUFRAKIS for their advice and support, and J. BILLEY and H. TOWNSEND for their field work at Palmer Station. This research was supported in part by the Division of Polar Programs of the National Science Foundation under grant DPP79-24600 A02, and in part by the Office of Naval Research under grant ONR N00014-76-C-0689.

REFERENCES

BUDDEN K. G.	1961	*Radio Waves in the Magnetosphere*, Cambridge University Press.
BULLOUGH K. and SAGREDO J. L.	1973	*Planet. Space Sci.* **21**, 899.
CARPENTER D. L. and MILLER T. R.	1976	*J. geophys. Res.* **81**, 2692.
CARPENTER D. L.	1980	*J. geophys. Res.* **85**, 4157.
HELLIWELL R. A. and KATSUFRAKIS J. P.	1978	*Antarctic Research Series*, Vol. 29.
LEAVITT M. K., CARPENTER D. L., SEELY N. T., PADDEN R. R. and DOOLITTLE J. H.	1978	*J. geophys. Res.* **83**, 1601.

MORGAN M. G. and EVANS R. W.	1951	*Proc. IRE* **39,** 553.
OKADA T., IWAI A. and HAYAKAWA M.	1977	*Planet. Space Sci.* **25,** 233.
RAGHURAM R. L., SMITH R. L. and BELL T. F.	1974	*IEEE Trans. Antennas Propagat.* **AP-22,** 334.
STRANGEWAYS H. J.	1980	*J. atmos. terr. Phys.* **42,** 995.
STRANGEWAYS H. J. and RYCROFT M. J.	1980	*J. atmos. terr. Phys.* **42,** 1009.
TSURUDA K. and HAYASHI K.	1975	*J. atmos. terr. Phys.* **37,** 1193.
WAIT J. R. and PERRY L. B.	1957	*J. geophys. Res.* **62,** 43.

Reference is also made to the following unpublished material:

BILLEY J.	1981	Personal communication.
COUSINS M. D.	1972	Technical Rep. No. 3432-2, Radioscience Lab., Stanford Univ., California.
CRARY J.	1961	Technical Rep. No. 9, Radioscience Lab., Stanford Univ., California.
LEAVITT M. K.	1975	Technical Rep. No. 3456-2, Radioscience Lab., Stanford Univ., California.
SEELY N. T.	1977	Technical Rep. No. 3742-1, Radioscience Lab., Stanford Univ., California.
STRANGEWAYS H. J.	1978	Ph.D. Thesis, Univ. of Southampton, U.K.